

# A Baseline for Multi-Label Image Classification Using Ensemble Deep CNN

Qian Wang

Ning Jia

Toby Breckon

Durham University

{qian.wang, ning.jia, toby.breckon}@durham.ac.uk

## Abstract

*Recent studies on multi-label image classification have been focusing on designing more complex architectures of deep neural networks such as the use of attention mechanism and region proposal networks. Although performance gains have been reported in literature, the backbone deep models of the proposed approaches and the evaluation metrics employed in different works vary, making it difficult to compare with each other fairly. Moreover, due to the lack of properly investigated baselines, the advantage introduced by the proposed techniques in literature are vague. To address these issues, we make a thorough investigation of the mainstream deep convolutional neural network architectures for multi-label image classification and present a strong baseline. With only data augmentation and model ensemble, we achieve better performance than those previously reported on three benchmark datasets. We hope the work presented in this paper will provide insights to the future studies on multi-label image classification.*

## 1. Introduction

The computer vision based image classification starts from recognising the principle concept within an image, generally labelled with its primary object. Through decades of comprehensive study on this essential subject, dramatic progress has been made towards a robust image classification framework with single-label output. Meanwhile, to pursue a comprehensive description of an image which often comprises far more diverse and substantial content and scene details, multi-label image classification (also known as multi-label annotation [19, 8]) has become a trending topic, whose extensive applications include but not limited to image retrieval, automatic image annotation, web image search and image tagging [9, 3, 39, 37].

The abundant labelled data (e.g. ImageNet [23]) and advanced computational hardware have promoted the development of deep convolutional neural network (CNN) [14, 13] based methods on single-label image classification. The self-adaptive reception fields and hierarchical

non-linear connections between layers offer CNN stronger feature extraction and better generalisation ability in learning representations. Further, by extending the depth of the network architecture, the recent deep models have significantly improved the performance on the benchmarking datasets with a reduced number of parameters [10]. Recently, such successful models have been extended to multi-label classification tasks with promising performance reported by [26, 29, 16, 40, 30, 33, 32], proving that CNN models are capable of handling this challenging and more general problem. However, due to the varying base models and specific optimization “tricks” employed in the experiments, approaches proposed in different literature cannot be directly compared with each other, obscuring their contributions. In addition, the lack of thoroughly investigated baselines of these deep CNN models hinders an explicit evaluation of the benefit brought by advanced frameworks specially designed for multi-label image classification.

A variety of evaluation metrics have been used in literature to compare the performance of different methods for multi-label image classification. We have observed that some commonly adopted evaluation metrics have been misused thus leading to unfair comparisons between different methods and making the reported performance less convincing. For example, the most commonly used *precision* and *recall* are correlated [5], one can tune the confidence threshold of predicted labels to achieve a high precision or recall for the same method. Therefore a higher precision or recall does not necessarily mean the method is superior.

To address the aforementioned issues, we intend to make a thorough investigation on different baseline deep CNN models and evaluation metrics for multi-label image classification. We focus on two state-of-the-art deep CNN architectures, i.e., VGG16 [40] and ResNet101[32], as they have been widely employed in multi-label image classification. While pointing out the drawbacks of some commonly used evaluation metrics for multi-label image classification, we propose reliable metrics for the performance evaluations of the baseline methods, providing a platform for direct comparisons between different approaches. Further, we present an evaluation benchmark by taking advantage of the data

augmentation and model ensemble, achieving better performance than the previously reported results on three benchmark datasets.

The main contributions of this paper are as follows:

- We investigate the baseline performance of different deep CNN models on three commonly used benchmark datasets for multi-label image classification. By using multiple data augmentation techniques during training and various model ensemble methods in the testing phase, we present a strong baseline performance that outperforms state-of-the-art techniques.
- We investigate different evaluation metrics for multi-label classification, discuss how they can be used to make fair comparisons between different models.

## 2. Related Work

In this section, we firstly introduce the topics related to multi-label image classification, presenting a global picture of multi-label classification and image understanding, as well as a clear idea how they are connected to other related research topics. Subsequently we briefly review recent progresses on multi-label image classification using deep convolutional neural networks.

### 2.1. Multi-Label Classification

In contrast to the traditional classification problem where only a single class label is attached to an instance, multi-label classification tackles a more realistic problem that each instance could be assigned with multiple labels to comprehensively represent its semantics. Multi-label classification has been applied in a variety of real-world applications including text categorization [18, 21], image/video understanding [26, 29, 16, 27], acoustic pattern recognition [34, 2], bioinformatics [20, 7] among others [25, 28]. Recent studies on multi-label classification mainly focus on the adaptation of single-label classification algorithms, the design of loss functions [16] for multi-label classification [8, 16] and the exploration of label correlations [38, 41]. A thorough review on conventional multi-label methods can be found in [36]. Apart from the development of new approaches to general multi-label classification problems, more methods are specially devised to address the domain specific issues in different multi-label classification applications. One typical research direction falling into this category is the feature extraction and selection [35] for specific multi-label data. As for multi-label images which usually contain multiple objects and semantic concepts in subregions, a good visual representation is essential to characterize the semantics comprehensively. One solution to learn visual representations from such multi-label images is the deep convolutional neural network which has shown great successes in many areas.

### 2.2. Multi-Label Image Classification

Other than simply describing multiple objects within an image, multi-label image classification conveys a comprehensive understanding of the image concept, i.e. its semantic meaning. On one hand, a success in multi-label image classification will benefit other tasks of image understanding including image captioning and image retrieval. On the other hand, multi-label image classification will benefit from tasks such as image segmentation and object detection.

Early works on multi-label image classification use hand-crafted image features and classifiers adapted to multi-label classification. TagProp [9] is an approach proposed by Guillaumin et al. using a weighted nearest-neighbor model to exploit multi-label training images. Matrix completion approach was proposed by Cabral et al. [1], assuming that the histogram based features of a multi-label image can be decomposed as a linear combination of multiple class histogram basis. The performance of these early works is restricted due to the poor ability of hand-crafted features in representing complex visual information in multi-label images.

Impressive progresses on multi-label image classification have been made by using deep convolutional neural networks. Wang et al. [26] proposed a CNN-RNN framework to explore the label co-occurrence using the long-short term memory (LSTM). Although VGG16 was employed for the CNN part, the model capacity was not fully exploited by fine-tuning the parameters. Zhang et al. [32] extended the idea by improving the CNN part. They proposed a regional latent semantic dependencies (RLSD) model for multi-label image classification, which focused on small objects in the multi-label images by generating subregions that potentially contain multiple objects and visual concepts. An LSTM based model was employed to generate multiple labels. Recently, the attention mechanism has been introduced to deep neural networks for multi-label image classification. It aims to explicitly or implicitly extract multiple visual representations from a single image characterizing different associated labels [29, 40]. Although improved performance has been reported by introducing more advanced frameworks, we notice that the performance of those proposed methods has marginal gains towards the vanilla deep models, and the training strategies employed in different works vary. Therefore it is necessary to set up a uniform baseline for comparison.

## 3. Method

We present the methods used to produce the strong baseline performance in this section. We first formulate the multi-label image classification problem; secondly we describe the employed deep convolutional neural networks adapted for multi-label classification, as well as the essen-

tial data augmentation techniques for training an improved deep model; then a simple yet effective model ensemble approach is introduced; and finally we investigate different evaluation methods for multi-label image classification.

### 3.1. Problem Formulation

Assume we have a set of training examples  $\mathcal{D} = \{(\mathbf{x}_i, \mathbf{y}_i)\}, i = 1, 2, \dots, n$ , where  $\mathbf{x}$  is an image,  $\mathbf{y} \in \{0, 1\}^C$  is the corresponding label vector,  $n$  and  $C$  are the numbers of training images and associated class labels respectively, the element values of zeros and ones in the label vector  $\mathbf{y}$  denote the absence and presence of the corresponding concepts in the image. The objective of multi-label image classification is to learn a model from the training data  $\mathcal{D}$ , such that for a given test image  $\hat{\mathbf{x}}$  we can use the learned model to predict its label vector  $\hat{\mathbf{y}}$ . In practice, most parametric models do not directly output a binary vector  $\hat{\mathbf{y}}$ , instead they predict a score vector  $\hat{\mathbf{s}} = f(\hat{\mathbf{x}}; \Theta) \in \mathbb{R}^C$  indicating the confidence of presence for each label.  $\hat{\mathbf{y}}$  can be derived from  $\hat{\mathbf{s}}$  by setting a threshold of confidence or the number of positive labels [16].

### 3.2. Base Model

Deep convolutional neural networks can be used to implement the model  $f(\mathbf{x}; \Theta)$  for multi-label image classification with an image  $\mathbf{x}$  as the input and a  $C$ -dimensional score vector  $\mathbf{s}$  as the output. In contrast to the traditional multi-label classification approaches, deep models integrate the feature extraction and classification in a single framework, enabling end-to-end learning. More importantly, state-of-the-art deep CNN models are able to learn high-level visual representations and approximate very complex learning systems.

**Model adaptation** We focus on two deep CNN architectures which have been used in multi-label image classification: VGG16 [24] and Resnet-101 [10] in our study. The deep CNN models are used to predict the score vector  $\mathbf{s}$  given an image. For this purpose, the final output layer for single-label classification in the original model is simply replaced with an additional fully connected layer in which the number of neurons is set as  $C$  (i.e. the number of concerned class labels).

**Loss function** We use the cross-entropy loss for model training. For a training example  $(\mathbf{x}_i, \mathbf{y}_i)$  and its predicted score vector  $\mathbf{s}_i = f(\mathbf{x}_i; \Theta)$ , the loss can be computed by the following equation:

$$loss(\mathbf{s}_i, \mathbf{y}_i) = - \sum_{j=1}^C (y_{ij} \cdot \log(\sigma(s_{ij})) + (1 - y_{ij}) \cdot \log(1 - \sigma(s_{ij}))), \quad (1)$$

where  $y_{ij}$  is the  $j$ -th element of the ground truth label vector  $\mathbf{y}_i$ ,  $s_{ij}$  is the  $j$ -th element of the predicted score vector  $\mathbf{s}_i$ , and  $\sigma(\cdot)$  is the sigmoid function  $\sigma(x) = 1/(1 + \exp(-x))$ .

**Data Augmentation** Data augmentation techniques have proven to benefit the training of deep models for single label image classification. We attempt to investigate how different data augmentation techniques affect the multi-label image classification. This is non-trivial since some commonly adopted data augmentation techniques such as random cropping will change the semantics in the original image. For example, a random cropping of a multi-label image might result in image patches not containing all the objects in the original image thus it is questionable whether they are still applicable to multi-label classification.

Apart from the conventional data augmentation techniques, we also adapt the *mixup* [31, 12] method to further increase data variability. Specifically, we randomly select two samples  $(\mathbf{x}_i, \mathbf{y}_i)$  and  $(\mathbf{x}_j, \mathbf{y}_j)$  from the mini-batch (the samples in a min-batches could be image patches cropped from the original images, resized to the same size). The mixed sample  $(\mathbf{x}, \mathbf{y})$  can be created in the following way:

$$\begin{aligned} \mathbf{x} &= (\mathbf{x}_i + \mathbf{x}_j)/2, \\ \mathbf{y} &= \mathbf{y}_i \vee \mathbf{y}_j, \end{aligned} \quad (2)$$

where the mixed image  $\mathbf{x}$  is created by a pixel-wise average on two original images and the corresponding label vector  $\mathbf{y}$  is obtained by an element-wise logical **OR** operation on  $\mathbf{y}_i$  and  $\mathbf{y}_j$ . During training, the *mixup* is alternately enabled and disabled for every epoch as suggested in [12]. We investigate the *mixup* technique due to the fact that it alters the target label combinations which are quite different from other traditional data augmentation techniques.

### 3.3. Model Ensemble

We use model ensemble techniques to improve the performance. A simple score level fusion method is employed during the testing phase. Suppose we have  $m$  score matrices  $\mathbf{S}_i, i = 1, 2, \dots, m$  predicted by  $m$  base models, the fused score matrix  $\mathbf{S}^{fusion}$  can be computed as follows:

$$\mathbf{S}^{fusion} = \frac{1}{m} \sum_{i=1}^m \mathbf{S}_i. \quad (3)$$

We explore and exploit three approaches to promote the diversity of base models hence improving the performance of model ensemble. Firstly, we investigate base models trained with different random seeds. Training deep CNN models using randomly shuffled mini-batches makes them converge to different local optimums, hence the resultant models will generate diverse predictions for the testing images. The combination of these base models have proven to be effective [11]. Secondly, we combine models trained without or with different data augmentation strategies. Specifically, we consider three different training strategies to obtain diverse trained models for the purpose of ensemble, i.e., training without data augmentation, training

with traditional data augmentation and training with *mixup*. Thirdly, we combine the models using different deep CNN architectures (e.g., VGG and ResNet).

### 3.4. Evaluation Methods

Evaluations metrics used for multi-label image classification can be categorized into three groups: image-centric, label-centric and overall metrics. Image-centric metrics evaluate the prediction accuracy for each image and calculate the average over all images, hence they are appropriate from the perspective of applications such as image tagging. Commonly used image-centric evaluation metrics include instance-centric mean average precision (I-MAP) [27], per-image precision (I-P), recall (I-R) and  $F_1$  score (I- $F_1$ ). Label-centric metrics evaluate the prediction accuracy in terms of each label and calculate the average over all labels, hence they are appropriate from the perspective of applications like image retrieval. Commonly used label-centric evaluation metrics include label-centric mean average precision (L-MAP)<sup>1</sup>, per-label (per-class) precision (L-P), recall (L-R) and  $F_1$  score (L- $F_1$ ). The evaluation metrics fallen into the third category include overall precision (O-P), recall (O-R) and  $F_1$  score (O- $F_1$ ).

According to [27], the definitions of I-MAP and L-MAP are based on the score matrix  $\mathbf{S} \in \mathbb{R}^{m \times C}$  involving all predictions of  $m$  test images for  $C$  labels. To calculate the precision, recall and  $F_1$  score, two approaches are employed. One is to reserve top- $k$  (e.g.,  $k = 3$ ) labels as the predictions for each test image according to the scores, the other is to reserve the labels whose scores are above a threshold  $t$  as the predictions. Top- $k$  overall precision, recall and  $F_1$  are reliable metrics used to compare different models, noting that they always increase simultaneously for a better model. In contrast, the precision and recall calculated by setting a threshold are less reliable, since the threshold values can affect the precision and recall values to a large extent. Specifically, a higher threshold will probably increase the precision by sacrificing the recall and a lower threshold will benefit the recall but lead to a dropped precision. With this regards, a model is not convincingly superior unless both the precision and recall are higher. As a result, the precision, recall and  $F_1$  obtained by setting a single threshold value are limited in evaluating a multi-label classification model. Alternatively, we can use a precision recall curve and the area under curve (AUC-PR) as reliable evaluation metrics. The precision recall curve can be obtained by setting the threshold to a set of different values.

In some literature [26, 29, 32], a threshold value is used to filter out some predicted labels of low scores when calculating the top- $k$  precision, recall and  $F_1$ . Since the number of predicted labels is allowed to be less than  $k$  for the images

<sup>1</sup>I-MAP and L-MAP are also named as MiAP and mAP in literature [37, 15]

with less than  $k$  ground truth positive labels, the precision can be improved without affecting the recall too much. Due to the same reason for the threshold based metrics, these modified top- $k$  precision, recall and  $F_1$  could also be biased as the evaluation metrics for model comparison.

Based on the above discussion, we suggest using the following evaluation metrics for multi-label image classification: I-MAP, L-MAP, per-label top- $k$  precision, recall,  $F_1$ , overall precision, recall,  $F_1$  and threshold based precision recall curve, and PR-AUC.

## 4. Experiments and Results

In this section, we describe our experiments on three benchmarks and report the experimental results. We introduce the datasets used in our experiments and the implementation details of the deep model training in the first two subsections respectively, then three experiments and their results are presented in the following three subsections.

### 4.1. Dataset

Table 1. A summary of datasets used in our experiments.

Dataset	# Labels	# Training Images	# Validation Images	# Test Images
NUS-WIDE[4]	81	90,804	10,089	67,742
MS-COCO[17]	80	73,873	8,208	40,137
VOC2007[6]	20	4,761	250	4,952

We use three benchmark datasets for multi-label image classification in our experiments, i.e., NUS-WIDE [4], MS-COCO [17] and VOC 2007 [6]. A summary of three datasets is presented in Table 4.

The **NUS-WIDE** dataset contained 269,648 images annotated with 81 labels. A large number of the images are no longer available now, thus we are only able to collect 168,635 images, among which 67,742 images are from the official testing subset, and 100,893 images are from the training subset. We randomly reserve 10% of the training images as validation data (i.e. 10,089 images) and the rest for training (i.e. 90,804 images).

The **MS-COCO** dataset contains a total of 122,218 images associated with 80 labels. We use the original training set, i.e., 82,783 images for training and validation. Again we randomly select 10% (i.e. 8,208) images as validation data and the rest of 73,873 images are used for training. The original validation set containing 40,137 images is used for testing.

The **VOC 2007** dataset contains 9,963 images from 20 object categories. We follow the original data split with 5,011 and 4,952 images for training/validation and testing respectively. Due to the relatively small number of training/validation images, we reserve random 5% (i.e. 250) of the 5,011 images for validation and the rest for training.

## 4.2. Implementation

All the deep CNN models used in our experiments are implemented in PyTorch [22]. We use the model weights pre-learned on the ImageNet for single-label image classification as the initialization and fine-tune the weights of all layers. We use the stochastic gradient descent (SGD) optimizer for model training with an initial learning rate of 0.1. The learning rate decays to one tenth when the validation loss stops decreasing for 5 epochs. We stop training when the learning rate has dropped to 0.0001 which takes less than 50 epochs for most cases.

## 4.3. Experiments on Data Augmentation

We investigate how data augmentation affects the performance of different deep CNN models. The models are trained without any data augmentation, with only traditional data augmentation (i.e. random cropping and horizontal flipping) and with both traditional data augmentation and data *mixup*. We do the experiments on three datasets using two deep CNN architectures. Each experiment is repeated for three times with different random seeds. We report the mean and standard deviation of the evaluation metrics over each group of three experimental results. The ensemble results will be presented in the following subsection.

The experimental results of using different data augmentation techniques are shown in Table 2. It is clear that the use of data augmentation significantly benefits the performance of both VGG16 [24] and ResNet101 [10] consistently on three benchmark datasets in terms of all the concerned evaluation metrics, except when the ResNet101 model is employed on the VOC2007 dataset where the use of traditional data augmentation does not make a big difference. By a comparison between the use of only traditional data augmentation (w/ HF+RC) and the joint use of traditional data augmentation and *mixup*, we can see that the later generates better performance in most cases. Comparing to VGG16, the ResNet101 models always perform better, which is consistent with their performance in single-label image classification.

## 4.4. Experiments on Model Ensemble

We explore the benefit brought by the ensemble of multiple base models and the effectiveness of three types of ensembles (c.f. section 3.3). In Table 3, we present the experimental results of three different ensemble approaches (i.e. En1, En2 and En3).

The first type of ensemble takes advantage of models training with different random seeds. The randomness in mini-batches promotes the diversity of trained models, making them complementary to each other. Three models are trained for each experimental setting with only the random seed varying, and the predictions are combined as the

final prediction by a simple average (c.f. Eq.(3)). By comparing Table 2 and 3, we can see that the ensemble of three models consistently achieves better performance.

The second type of ensemble is based on the models trained using different data augmentation strategies. Since we have trained three base models for each training strategy, the ensemble of three strategies is actually a combination of nine base models in terms of their predicted score matrices during the testing phase. Again, performance improvement can be observed from Table 3. By a close look at Table 3 we can draw the following conclusions. Firstly, the second type of ensemble achieves better performance in terms of L-MAP, I-MAP and overall precision (O-P), recall (O-R),  $F_1$  (O- $F_1$ ) for most cases. However, it does not help to improve the label-centric metrics, i.e., L-P, L-R and L- $F_1$ . Secondly, we can see that the relation between top- $k$  based overall precision and recall is monotonic, while the relation between label-centric ones is not.

We also investigate a third type of ensemble by combining results of models with different CNN architectures (e.g., VGG16 and ResNet101). The performance can be slightly improved for NUSWIDE and VOC2007 datasets, but for the MS-COCO dataset, the ensemble of VGG16 and ResNet101 performs no better than ResNet101 itself. The reason is ResNet101 performs much better than VGG16 on MS-COCO in single-label classification task, indicating enhanced feature learning ability on this specific dataset.

Overall the results in Table 3 demonstrate the effectiveness of two types of ensembles for both deep CNN architectures on three benchmark datasets.

## 4.5. Comparative Study

We compare the proposed approaches with state-of-the-arts. We consider the most recently published approaches using deep CNN models with competitive performance reported. Specifically, the following methods are selected for the comparison:

- **CNN-RNN**[26] used the pre-trained VGG16 as the backbone for the CNN part without fine-tuning, leading to the inferior performance.
  - **WARP**, **Ranking** and **LSEP** are three implementations of multi-label classification loss functions by Li et al. [16], using fine-tuned VGG16.
  - **RLSD** [32] is a new multi-label image classification model with the exploration of regional latent semantic dependencies. VGG16 is used as the backbone CNN with fine-tuning employed.
  - **AttRegion**[29] is able to discover semantic-aware regions using a VGG16 based visual attention model.
  - **ResNet-SRN**[40] is a leading approach for multi-label image classification using ResNet101. Again an attention model is employed as the spatial regularization.
- To make a fair comparison, we categorize the meth-

Table 2. Experimental results of data augmentation (DA) on three benchmark datasets. We report the mean  $\pm$  std of L-MAP, I-MAP, top-3 per-label and overall precision, recall,  $F_1$ . HF and RC denote the traditional data augmentation using horizontal flipping and random cropping respectively.

Dataset	Base Model Type	Method	L-MAP	I-MAP	L-P	L-R	L-F <sub>1</sub>	O-P	O-R	O-F <sub>1</sub>
NUS-WIDE	VGG16	w/o DA	55.2 $\pm$ 0.3	82.0 $\pm$ 0.2	44.7 $\pm$ 0.9	51.2 $\pm$ 1.0	43.8 $\pm$ 0.8	55.0 $\pm$ 0.1	67.7 $\pm$ 0.1	60.7 $\pm$ 0.1
		w/ HF	56.1 $\pm$ 0.3	82.2 $\pm$ 0.0	44.3 $\pm$ 1.0	52.2 $\pm$ 0.7	44.5 $\pm$ 1.5	55.2 $\pm$ 0.0	67.9 $\pm$ 0.0	60.9 $\pm$ 0.0
		w/ RC	57.2 $\pm$ 0.3	82.4 $\pm$ 0.2	44.9 $\pm$ 0.2	54.4 $\pm$ 0.2	46.1 $\pm$ 0.2	55.3 $\pm$ 0.1	68.0 $\pm$ 0.1	61.0 $\pm$ 0.1
		w/ HF+RC	<b>58.0 <math>\pm</math> 0.1</b>	82.8 $\pm$ 0.1	<b>45.5 <math>\pm</math> 0.3</b>	<b>55.0 <math>\pm</math> 0.3</b>	46.1 $\pm$ 0.2	55.5 $\pm$ 0.0	68.3 $\pm$ 0.0	61.2 $\pm$ 0.0
		w/ HF+RC+mixup	57.8 $\pm$ 0.5	<b>83.0 <math>\pm</math> 0.2</b>	<b>45.5 <math>\pm</math> 0.1</b>	54.4 $\pm$ 0.8	<b>46.4 <math>\pm</math> 0.4</b>	<b>55.7 <math>\pm</math> 0.1</b>	<b>68.6 <math>\pm</math> 0.1</b>	<b>61.5 <math>\pm</math> 0.1</b>
	ResNet101	w/o DA	56.7 $\pm$ 0.2	82.5 $\pm$ 0.1	46.1 $\pm$ 1.1	53.4 $\pm$ 1.8	46.1 $\pm$ 0.6	55.3 $\pm$ 0.1	68.1 $\pm$ 0.1	61.0 $\pm$ 0.1
		w/ HF	56.9 $\pm$ 0.8	82.6 $\pm$ 0.2	46.3 $\pm$ 1.1	53.0 $\pm$ 1.4	46.4 $\pm$ 0.5	55.4 $\pm$ 0.1	68.2 $\pm$ 0.1	61.1 $\pm$ 0.1
		w/ RC	59.4 $\pm$ 0.2	82.9 $\pm$ 0.2	47.0 $\pm$ 0.3	56.5 $\pm$ 0.4	48.1 $\pm$ 0.3	55.6 $\pm$ 0.1	68.5 $\pm$ 0.1	61.4 $\pm$ 0.1
		w/ HF+RC	<b>59.5 <math>\pm</math> 0.2</b>	83.0 $\pm$ 0.1	47.0 $\pm$ 0.3	<b>56.7 <math>\pm</math> 0.4</b>	48.0 $\pm$ 0.3	55.7 $\pm$ 0.0	68.6 $\pm$ 0.0	61.5 $\pm$ 0.0
		w/ HF+RC+mixup	59.3 $\pm$ 0.1	<b>83.2 <math>\pm</math> 0.1</b>	<b>47.5 <math>\pm</math> 0.7</b>	55.8 $\pm$ 0.1	<b>48.5 <math>\pm</math> 0.4</b>	<b>55.9 <math>\pm</math> 0.1</b>	<b>68.8 <math>\pm</math> 0.1</b>	<b>61.7 <math>\pm</math> 0.1</b>
MS-COCO	VGG16	w/o DA	68.4 $\pm$ 0.3	82.9 $\pm$ 0.2	55.0 $\pm$ 1.5	58.5 $\pm$ 0.4	55.7 $\pm$ 1.1	60.9 $\pm$ 0.1	62.9 $\pm$ 0.1	61.9 $\pm$ 0.1
		w/ HF	70.2 $\pm$ 0.2	84.0 $\pm$ 0.1	57.1 $\pm$ 1.3	59.7 $\pm$ 0.7	57.3 $\pm$ 0.6	61.9 $\pm$ 0.1	63.9 $\pm$ 0.1	62.9 $\pm$ 0.1
		w/ RC	71.9 $\pm$ 0.1	85.3 $\pm$ 0.1	61.2 $\pm$ 0.6	60.3 $\pm$ 0.0	60.4 $\pm$ 0.6	63.0 $\pm$ 0.1	65.0 $\pm$ 0.1	64.0 $\pm$ 0.1
		w/ HF+RC	<b>72.9 <math>\pm</math> 0.1</b>	<b>85.9 <math>\pm</math> 0.1</b>	<b>62.0 <math>\pm</math> 0.5</b>	<b>60.9 <math>\pm</math> 0.1</b>	<b>60.8 <math>\pm</math> 0.3</b>	<b>63.4 <math>\pm</math> 0.0</b>	<b>65.5 <math>\pm</math> 0.0</b>	<b>64.4 <math>\pm</math> 0.0</b>
		w/ HF+RC+mixup	71.7 $\pm$ 0.6	85.3 $\pm$ 0.4	61.9 $\pm$ 0.7	59.8 $\pm$ 0.3	60.4 $\pm$ 0.4	62.8 $\pm$ 0.3	64.8 $\pm$ 0.3	63.8 $\pm$ 0.3
	ResNet101	w/o DA	71.4 $\pm$ 0.4	84.8 $\pm$ 0.1	59.6 $\pm$ 2.2	60.4 $\pm$ 0.6	59.0 $\pm$ 0.8	62.5 $\pm$ 0.3	64.6 $\pm$ 0.3	63.5 $\pm$ 0.3
		w/ HF	73.2 $\pm$ 0.3	85.8 $\pm$ 0.2	60.8 $\pm$ 1.2	61.5 $\pm$ 0.1	59.7 $\pm$ 0.3	63.4 $\pm$ 0.1	65.5 $\pm$ 0.1	64.5 $\pm$ 0.1
		w/ RC	74.3 $\pm$ 0.2	86.7 $\pm$ 0.1	65.0 $\pm$ 0.5	61.9 $\pm$ 0.2	61.8 $\pm$ 0.2	64.2 $\pm$ 0.1	66.3 $\pm$ 0.1	65.2 $\pm$ 0.1
		w/ HF+RC	74.6 $\pm$ 0.4	86.8 $\pm$ 0.3	64.6 $\pm$ 0.6	62.2 $\pm$ 0.2	62.2 $\pm$ 0.7	64.3 $\pm$ 0.2	66.4 $\pm$ 0.2	65.4 $\pm$ 0.2
		w/ HF+RC+mixup	<b>75.5 <math>\pm</math> 0.1</b>	<b>87.5 <math>\pm</math> 0.1</b>	<b>65.8 <math>\pm</math> 0.4</b>	<b>62.8 <math>\pm</math> 0.2</b>	<b>63.7 <math>\pm</math> 0.5</b>	<b>64.8 <math>\pm</math> 0.0</b>	<b>67.0 <math>\pm</math> 0.0</b>	<b>65.9 <math>\pm</math> 0.0</b>
VOC2007	VGG16	w/o DA	83.5 $\pm$ 0.2	90.3 $\pm$ 0.2	40.1 $\pm$ 0.5	86.7 $\pm$ 0.3	54.0 $\pm$ 0.4	45.3 $\pm$ 0.1	88.1 $\pm$ 0.2	59.8 $\pm$ 0.1
		w/ HF	84.2 $\pm$ 0.7	91.2 $\pm$ 0.3	38.9 $\pm$ 0.2	89.6 $\pm$ 0.3	53.5 $\pm$ 0.3	43.1 $\pm$ 0.1	91.4 $\pm$ 0.2	58.6 $\pm$ 0.1
		w/ RC	84.9 $\pm$ 0.5	92.0 $\pm$ 0.2	45.3 $\pm$ 0.7	89.4 $\pm$ 0.5	59.0 $\pm$ 0.7	43.5 $\pm$ 0.2	92.1 $\pm$ 0.4	59.1 $\pm$ 0.2
		w/ HF+RC	85.3 $\pm$ 0.3	91.7 $\pm$ 0.2	<b>47.2 <math>\pm</math> 0.2</b>	87.1 $\pm$ 0.4	<b>60.5 <math>\pm</math> 0.3</b>	46.2 $\pm$ 0.1	89.9 $\pm$ 0.3	61.0 $\pm$ 0.2
		w/ HF+RC+mixup	<b>86.7 <math>\pm</math> 0.3</b>	<b>92.9 <math>\pm</math> 0.3</b>	43.8 $\pm$ 0.7	<b>89.0 <math>\pm</math> 0.6</b>	58.0 $\pm$ 0.4	<b>46.6 <math>\pm</math> 0.2</b>	<b>90.7 <math>\pm</math> 0.3</b>	<b>61.5 <math>\pm</math> 0.2</b>
	ResNet101	w/o DA	85.5 $\pm$ 0.2	91.7 $\pm$ 0.2	40.7 $\pm$ 0.2	87.8 $\pm$ 0.0	55.0 $\pm$ 0.2	45.9 $\pm$ 0.1	89.3 $\pm$ 0.3	60.6 $\pm$ 0.2
		w/ HF	85.2 $\pm$ 0.0	91.9 $\pm$ 0.2	39.8 $\pm$ 0.7	89.9 $\pm$ 0.2	54.7 $\pm$ 0.7	43.4 $\pm$ 0.1	92.0 $\pm$ 0.2	59.0 $\pm$ 0.1
		w/ RC	83.4 $\pm$ 0.4	90.9 $\pm$ 0.2	43.6 $\pm$ 0.2	88.8 $\pm$ 0.7	57.6 $\pm$ 0.3	43.2 $\pm$ 0.2	91.4 $\pm$ 0.4	58.7 $\pm$ 0.2
		w/ HF+RC	84.5 $\pm$ 0.4	91.1 $\pm$ 0.4	<b>46.7 <math>\pm</math> 0.6</b>	86.8 $\pm$ 0.6	<b>60.0 <math>\pm</math> 0.5</b>	46.0 $\pm$ 0.2	89.5 $\pm$ 0.3	60.7 $\pm$ 0.2
		w/ HF+RC+mixup	<b>86.1 <math>\pm</math> 0.3</b>	<b>92.5 <math>\pm</math> 0.2</b>	46.0 $\pm$ 0.7	<b>87.9 <math>\pm</math> 0.2</b>	59.8 $\pm$ 0.5	<b>46.5 <math>\pm</math> 0.1</b>	<b>90.5 <math>\pm</math> 0.2</b>	<b>61.4 <math>\pm</math> 0.1</b>

Table 3. Experimental results of model ensemble on three benchmark datasets. We report the value of L-MAP, I-MAP, top-3 per-label and overall precision, recall,  $F_1$ . En1, En2 and En3 denote three types of ensemble approaches described in Section 3.3, respectively. Other notations are identical to those in Table 2.

Dataset	Base Model Type	Method	L-MAP	I-MAP	L-P	L-R	L-F <sub>1</sub>	O-P	O-R	O-F <sub>1</sub>
NUS-WIDE	VGG16	w/o DA (En1)	57.1	83.2	45.8	52.2	45.0	55.7	68.6	61.5
		w/ HF+RC (En1)	59.3	83.3	46.1	<b>55.5</b>	<b>47.4</b>	55.9	68.8	61.7
		w/ HF+RC+mixup (En1)	58.9	83.4	46.3	54.8	47.0	56.0	68.9	61.8
		En2	<b>60.2</b>	<b>84.0</b>	<b>47.5</b>	54.9	47.2	<b>56.4</b>	<b>69.4</b>	<b>62.2</b>
		En3	63.1	84.9	50.2	57.2	50.0	57.0	70.1	62.8
	ResNet101	w/o DA (En1)	59.1	84.0	47.7	55.0	47.9	56.3	69.3	62.1
		w/ HF+RC (En1)	61.6	83.9	49.0	<b>57.5</b>	49.0	56.3	69.3	62.1
		w/ HF+RC+mixup (En1)	61.0	83.9	49.0	56.3	49.4	56.3	69.3	62.1
		En2	<b>62.3</b>	<b>84.5</b>	<b>49.1</b>	<b>57.5</b>	<b>49.8</b>	<b>56.7</b>	<b>69.8</b>	<b>62.6</b>
		En3	63.1	84.9	50.2	57.2	50.0	57.0	70.1	62.8
MS-COCO	VGG16	w/o DA (En1)	70.5	84.4	56.0	59.8	58.0	62.1	64.2	63.1
		w/ HF+RC (En1)	<b>74.1</b>	86.7	<b>62.9</b>	61.5	<b>61.4</b>	<b>64.1</b>	<b>66.2</b>	<b>65.1</b>
		w/ HF+RC+mixup (En1)	72.2	85.7	62.4	60.1	60.8	63.1	65.2	64.1
		En2	<b>74.1</b>	<b>86.8</b>	61.5	<b>61.7</b>	60.7	<b>64.1</b>	<b>66.2</b>	<b>65.1</b>
		En3	76.5	88.2	63.6	63.2	63.5	65.3	67.5	66.4
	ResNet101	w/o DA (En1)	74.6	87.0	62.5	62.3	61.3	64.4	66.5	65.4
		w/ HF+RC (En1)	76.4	88.0	66.7	63.2	63.2	65.3	67.4	66.3
		w/ HF+RC+mixup (En1)	76.9	88.4	<b>68.4</b>	63.5	<b>64.7</b>	65.6	67.7	66.6
		En2	<b>77.9</b>	<b>88.9</b>	67.9	<b>64.0</b>	<b>64.7</b>	<b>66.0</b>	<b>68.2</b>	<b>67.1</b>
		En3	76.5	88.2	63.6	63.2	63.5	65.3	67.5	66.4
VOC2007	VGG16	w/o DA (En1)	85.5	91.5	40.5	88.2	54.8	45.9	89.4	60.7
		w/ HF+RC (En1)	85.5	91.5	40.5	88.2	54.8	45.9	89.4	60.7
		w/ HF+RC+mixup (En1)	87.2	93.2	43.9	89.4	58.3	46.8	91.1	61.8
		En2	<b>87.8</b>	<b>93.4</b>	<b>43.9</b>	<b>89.5</b>	<b>58.4</b>	<b>46.9</b>	<b>91.3</b>	<b>62.0</b>
		En3	89.4	94.3	46.3	90.3	60.8	47.4	92.3	62.6
	ResNet101	w/o DA (En1)	87.7	93.0	41.5	89.5	56.2	46.7	90.9	61.7
		w/ HF+RC (En1)	86.6	92.4	<b>48.3</b>	87.9	<b>61.6</b>	46.5	90.5	61.4
		w/ HF+RC+mixup (En1)	87.8	93.3	47.5	89.1	61.4	47.0	91.4	62.0
		En2	<b>88.9</b>	<b>94.0</b>	46.5	<b>90.0</b>	60.9	<b>47.2</b>	<b>91.9</b>	<b>62.4</b>
		En3	89.4	94.3	46.3	90.3	60.8	47.4	92.3	62.6

ods into two groups using VGG16 and ResNet101 as the backbone deep CNN models. The performance of different methods along with ours in terms of L-MAP, I-MAP and top-3 label-centric/overall precision, recall,  $F_1$  are pre-

sented in Table 4. On the other hand, we present the comparison of threshold based metrics in Figure 1. It is noteworthy that, in some literature, the top-3 precision and recall are calculated with additional restrictions of the predictions to

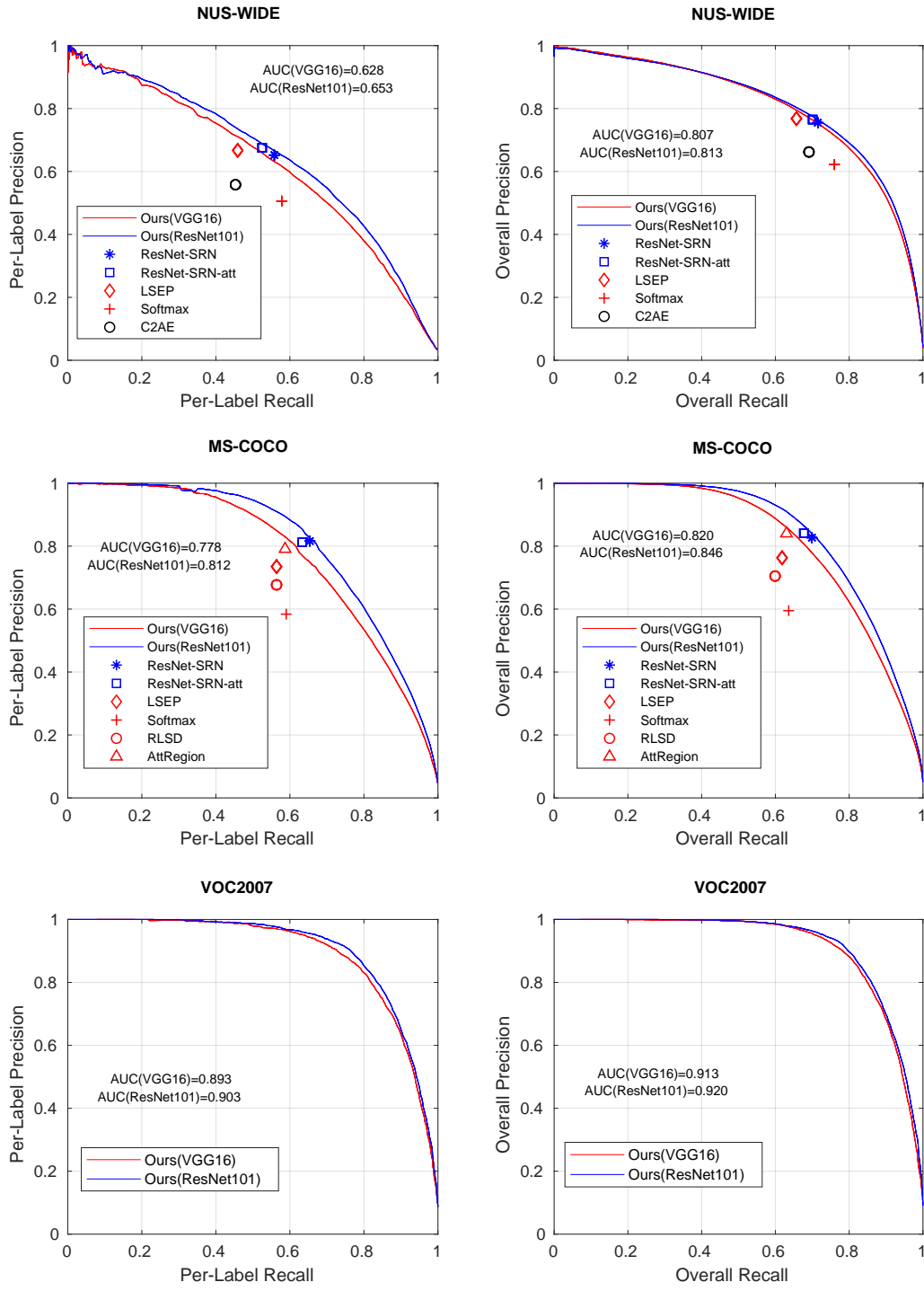


Figure 1. Comparison with state-of-the-art methods in terms of threshold based precision and recall. The methods using VGG16 and ResNet101 as the backbones are denoted with red and blue lines or markers respectively. The precision recall curves are based on our second type of ensemble models (En2) for the comparison with other methods which are denoted with different markers.

Table 4. Comparison with state-of-the-art results on three benchmark datasets. The precision, recall and  $F_1$  are based on top-3 predictions without any threshold conditions.

Dataset	Base Model Type	Method	L-MAP	I-MAP	L-P	L-R	L-F <sub>1</sub>	O-P	O-R	O-F <sub>1</sub>
NUS-WIDE	VGG16	CNN-RNN [26]	-	-	40.5	30.4	34.7	49.9	61.7	55.2
	VGG16	RLSD [32]	54.1	-	44.4	49.6	46.9	54.4	67.6	60.3
	VGG16	WARP [16]	-	-	43.8	<b>57.1</b>	-	54.5	67.9	60.5
	VGG16	Ours-Single	57.8	83.0	45.5	54.4	46.4	55.7	68.6	61.5
	VGG16	Ours-En2	<b>60.2</b>	<b>84.0</b>	<b>47.5</b>	54.9	<b>47.2</b>	<b>56.4</b>	<b>69.4</b>	<b>62.2</b>
	ResNet101	ResNet-SRN-att [40]	61.8	-	47.4	57.7	47.7	56.2	69.6	62.2
	ResNet101	ResNet-SRN [40]	62.0	-	48.2	<b>58.9</b>	48.9	56.2	69.6	62.2
	ResNet101	Ours-Single	59.3	83.2	47.5	55.8	48.5	55.9	68.8	61.7
ResNet101	Ours-En2	<b>62.3</b>	<b>84.5</b>	<b>49.1</b>	57.5	<b>49.8</b>	<b>56.7</b>	<b>69.8</b>	<b>62.6</b>	
MS-COCO	VGG16	WARP [16]	-	-	55.5	57.4	-	59.6	61.5	60.5
	VGG16	Ranking [16]	-	-	57.0	57.8	-	60.2	62.2	61.2
	VGG16	RLSD [32]	67.4	-	-	-	-	-	-	-
	VGG16	Ours-Single	72.9	85.9	<b>62.0</b>	60.9	<b>60.8</b>	63.4	65.5	64.4
	VGG16	Ours-En2	<b>74.1</b>	<b>86.8</b>	61.5	<b>61.7</b>	60.7	<b>64.1</b>	<b>66.2</b>	<b>65.1</b>
	ResNet101	ResNet-SRN [40]	77.1	-	-	-	-	-	-	-
	ResNet101	Ours-Single	75.5	87.5	65.8	62.8	63.7	64.8	67.0	65.9
	ResNet101	Ours-En2	<b>77.9</b>	<b>88.9</b>	<b>67.9</b>	<b>64.0</b>	<b>64.7</b>	<b>66.0</b>	<b>68.2</b>	<b>67.1</b>
VOC2007	VGG16	CNN-RNN [26]	84.0	-	-	-	-	-	-	-
	VGG16	AttRegion[29]	<b>91.9</b>	-	-	-	-	-	-	-
	VGG16	RLSD [32]	87.3	-	<b>50.5</b>	<b>90.6</b>	<b>64.9</b>	<b>47.5</b>	<b>92.4</b>	<b>62.7</b>
	VGG16	Ours-Single	86.7	92.9	43.8	89.0	58.0	46.6	90.7	61.5
	VGG16	Ours-En2	87.8	<b>93.4</b>	43.9	89.5	58.4	46.9	91.3	62.0
	ResNet101	Ours-Single	86.1	92.5	46.0	87.9	59.8	46.5	90.5	61.4
	ResNet101	Ours-En2	<b>88.9</b>	<b>94.0</b>	<b>46.5</b>	<b>90.0</b>	<b>60.9</b>	<b>47.2</b>	<b>91.9</b>	<b>62.4</b>

improve the precision (e.g., the positive predictions are required to be greater than a threshold). Thus it is unfair to compare them directly with the true top- $k$  based metrics. As a result, the reported results which are computed using the joint use of top- $k$  and threshold conditions are compared in Figure 1 instead of Table 4.

In terms of L-MAP, an evaluation metric based on the ranking list of all labels, our simple ensemble model performs the best on both NUS-WIDE and MS-COCO datasets using either VGG16 or ResNet101. In terms of overall precision, recall and  $F_1$ , our ensemble model also outperforms state-of-the-arts on two large-scale datasets. On the NUS-WIDE dataset, both the VGG16 and ResNet101 fail to rank at the top of the list in terms of label-centric recall, though they generate the highest label-centric precision as well as the  $F_1$ . As for the VOC2007 dataset, our investigated baseline method under-performs the RLSD and AttRegion approaches which employs attentional region proposal networks for the awareness of small objects. One reasonable explanation that our ensemble model is not superior is that the VOC2007 dataset is relatively small and inadequate for training a deep neural networks like VGG16 and ResNet101.

Figure 1 presents a comparison between our VGG16/ResNet101 based ensemble models and state-of-the-art methods in terms of threshold based precision, recall and  $F_1$ . As we discussed above, a single pair of threshold based precision and recall is inadequate for the comparison between different models since the precision and recall are affected by the values of threshold. As a result, we present the precision recall curve (PR curve) in Figure 1 together with the recall-precision pairs reported in literature. Specifically, we set the threshold to different

values of a large range and compute the corresponding precision and recall, leading to the precision recall curve. When the same backbone architecture (i.e. VGG16 or ResNet101) is used, the state-of-the-art performance are always under the PR curves of our models, which means our ensemble models outperform state-of-the-arts in terms of threshold based metrics. Besides, the area under PR curve is computed and presented in each subgraph.

Overall the the investigated ensemble models trained with data augmentation techniques perform better than the state-of-the-art techniques, setting a new strong baseline for multi-label image classification.

## 5. Conclusion

In summary, we investigated the use of different deep CNN models for multi-label image classification and present a simple yet effective ensemble model, achieving state-of-the-art performance on three benchmark datasets. The extensive experiments presented in this paper demonstrate the capabilities of deep CNN models in exploring the complex semantics in multi-label images. A good training strategy (e.g., fine-tuning all layers instead of using pre-learned weights, using data augmentation during training) is necessary to make the most of the deep models.

We also investigated different evaluation metrics for multi-label classification, discussed how they can be used for a fair comparison between different models. We reported our experimental results in terms of various evaluation metrics, presenting a strong baseline performance. We hope the experimental results in this paper will provide an insight for the future studies in multi-label image classification.

## References

- [1] R. Cabral, F. De la Torre, J. P. Costeira, and A. Bernardino. Matrix completion for weakly-supervised multi-label image classification. *IEEE transactions on pattern analysis and machine intelligence*, 37(1):121–135, 2015.
- [2] E. Cakir, T. Heittola, H. Huttunen, and T. Virtanen. Polyphonic sound event detection using multi label deep neural networks. In *IJCNN*, pages 1–7. IEEE, 2015.
- [3] M. Chen, A. Zheng, and K. Weinberger. Fast image tagging. In *ICML*, pages 1274–1282, 2013.
- [4] T.-S. Chua, J. Tang, R. Hong, H. Li, Z. Luo, and Y. Zheng. Nus-wide: a real-world web image database from national university of singapore. In *ACM international conference on image and video retrieval*, page 48. ACM, 2009.
- [5] J. Davis and M. Goadrich. The relationship between precision-recall and roc curves. In *ICML*, pages 233–240. ACM, 2006.
- [6] M. Everingham, L. Van Gool, C. K. Williams, J. Winn, and A. Zisserman. The pascal visual object classes (voc) challenge. *IJCV*, 88(2):303–338, 2010.
- [7] S. Fodeh, A. Tiwari, and H. Yu. Exploiting pubmed for protein molecular function prediction via nmf based multi-label classification. In *ICDMW*, pages 446–451. IEEE, 2017.
- [8] Y. Gong, Y. Jia, T. Leung, A. Toshev, and S. Ioffe. Deep convolutional ranking for multilabel image annotation. In *ICLR*, 2014.
- [9] M. Guillaumin, T. Mensink, J. Verbeek, and C. Schmid. Tagprop: Discriminative metric learning in nearest neighbor models for image auto-annotation. In *ICCV*, pages 309–316. IEEE, 2009.
- [10] K. He, X. Zhang, S. Ren, and J. Sun. Deep residual learning for image recognition. In *CVPR*, pages 770–778, 2016.
- [11] G. Huang, Y. Li, G. Pleiss, Z. Liu, J. E. Hopcroft, and K. Q. Weinberger. Snapshot ensembles: Train 1, get m for free. In *ICLR*, 2017.
- [12] H. Inoue. Data augmentation by pairing samples for images classification. *arXiv preprint arXiv:1801.02929*, 2018.
- [13] A. Krizhevsky, I. Sutskever, and G. E. Hinton. Imagenet classification with deep convolutional neural networks. In *NIPS*, pages 1097–1105, 2012.
- [14] Y. LeCun, L. Bottou, Y. Bengio, and P. Haffner. Gradient-based learning applied to document recognition. *Proceedings of the IEEE*, 86(11):2278–2324, 1998.
- [15] X. Li, T. Uricchio, L. Ballan, M. Bertini, C. G. Snoek, and A. D. Bimbo. Socializing the semantic gap: A comparative survey on image tag assignment, refinement, and retrieval. *ACM Computing Surveys (CSUR)*, 49(1):14, 2016.
- [16] Y. Li, Y. Song, and J. Luo. Improving pairwise ranking for multi-label image classification. In *CVPR*, pages 3617–3625, 2017.
- [17] T.-Y. Lin, M. Maire, S. Belongie, J. Hays, P. Perona, D. Ramanan, P. Dollár, and C. L. Zitnick. Microsoft coco: Common objects in context. In *ECCV*, pages 740–755. Springer, 2014.
- [18] S. M. Liu and J.-H. Chen. A multi-label classification based approach for sentiment classification. *Expert Systems with Applications*, 42(3):1083–1093, 2015.
- [19] H. Lu, Y. Zheng, X. Xue, and Y. Zhang. Content and context-based multi-label image annotation. In *CVPR-W*, pages 61–68. IEEE, 2009.
- [20] J. Meng, G.-L. Shi, and Y.-S. Luan. Plant mirna function prediction based on functional similarity network and transductive multi-label classification algorithm. *Neurocomputing*, 179:283–289, 2016.
- [21] J. Nam, J. Kim, E. L. Mencía, I. Gurevych, and J. Fürnkranz. Large-scale multi-label text classification revisiting neural networks. In *ECML-PKDD*, pages 437–452. Springer, 2014.
- [22] A. Paszke, S. Gross, S. Chintala, G. Chanan, E. Yang, Z. DeVito, Z. Lin, A. Desmaison, L. Antiga, and A. Lerer. Automatic differentiation in pytorch. In *NIPS-W*, 2017.
- [23] O. Russakovsky, J. Deng, H. Su, J. Krause, S. Satheesh, S. Ma, Z. Huang, A. Karpathy, A. Khosla, M. Bernstein, et al. Imagenet large scale visual recognition challenge. *IJCV*, 115(3):211–252, 2015.
- [24] K. Simonyan and A. Zisserman. Very deep convolutional networks for large-scale image recognition. In *ICLR*, 2015.
- [25] S. M. Tabatabaei, S. Dick, and W. Xu. Toward non-intrusive load monitoring via multi-label classification. *IEEE Transactions on Smart Grid*, 8(1):26–40, 2017.
- [26] J. Wang, Y. Yang, J. Mao, Z. Huang, C. Huang, and W. Xu. Cnn-rnn: A unified framework for multi-label image classification. In *CVPR*, pages 2285–2294. IEEE, 2016.
- [27] Q. Wang and K. Chen. Multi-label zero-shot human action recognition via joint latent embedding. *arXiv preprint arXiv:1709.05107*, 2017.
- [28] Y. Wang, E. Coiera, W. Runciman, and F. Magrabi. Automating the identification of patient safety incident reports using multi-label classification. *Studies*

*in health technology and informatics*, 245:609–613, 2017.

- [29] Z. Wang, T. Chen, G. Li, R. Xu, and L. Lin. Multi-label image recognition by recurrently discovering attentional regions. In *ICCV*, 2017.
- [30] C.-K. Yeh, W.-C. Wu, W.-J. Ko, and Y.-C. F. Wang. Learning deep latent space for multi-label classification. In *AAAI*, pages 2838–2844, 2017.
- [31] H. Zhang, M. Cisse, Y. N. Dauphin, and D. Lopez-Paz. mixup: Beyond empirical risk minimization. In *ICLR*, 2018.
- [32] J. Zhang, Q. Wu, C. Shen, J. Zhang, and J. Lu. Multi-label image classification with regional latent semantic dependencies. *IEEE Transactions on Multimedia*, 2018.
- [33] J. Zhang, Q. Wu, J. Zhang, C. Shen, and J. Lu. Kill two birds with one stone: Weakly-supervised neural network for image annotation and tag refinement. In *AAAI*, 2018.
- [34] L. Zhang, M. Towsey, J. Xie, J. Zhang, and P. Roe. Using multi-label classification for acoustic pattern detection and assisting bird species surveys. *Applied Acoustics*, 110:91–98, 2016.
- [35] M.-L. Zhang and L. Wu. Lift: Multi-label learning with label-specific features. *IEEE transactions on PAMI*, 37(1):107–120, 2015.
- [36] M.-L. Zhang and Z.-H. Zhou. A review on multi-label learning algorithms. *IEEE transactions on knowledge and data engineering*, 26(8):1819–1837, 2014.
- [37] Y. Zhang, B. Gong, and M. Shah. Fast zero-shot image tagging. In *CVPR*, pages 5985–5994. IEEE, 2016.
- [38] K. Zhao, W.-S. Chu, F. De la Torre, J. F. Cohn, and H. Zhang. Joint patch and multi-label learning for facial action unit detection. In *CVPR*, pages 2207–2216. IEEE, 2015.
- [39] N. Zhou, W. K. Cheung, G. Qiu, and X. Xue. A hybrid probabilistic model for unified collaborative and content-based image tagging. *IEEE Transactions on PAMI*, 33(7):1281–1294, 2011.
- [40] F. Zhu, H. Li, W. Ouyang, N. Yu, and X. Wang. Learning spatial regularization with image-level supervisions for multi-label image classification. In *CVPR*, pages 5513–5522, 2017.
- [41] Y. Zhu, J. T. Kwok, and Z.-H. Zhou. Multi-label learning with global and local label correlation. *IEEE Transactions on Knowledge and Data Engineering*, 2017.